Preparation of dense SnO_2-based ceramics by Fe_2O_3 addition

Masahiro YASUKAWA[*1] and Naoya MATSUOKA[*2]

[*1] *Department of Social Design Engineering, National Institute of Technology, Kochi College, 200-1 Monobe, Nankoku 783-8508, Japan*

[*2] *Department of Materials Science and Engineering, National Institute of Technology, Kochi College, 200-1 Monobe, Nankoku 783-8508, Japan*

Abstract

Dense SnO_2-based ceramics have been prepared by firing Fe_2O_3-added SnO_2 compacts with atomic ratio x = Fe/(Sn+Fe) = 0.005 − 0.10 at 1673 K. The densification is remarkably promoted even with the addition of a small amount of x = 0.005. The XRD results suggest that Fe^{3+} ions are doped into Sn^{4+} sites of the rutile-type structure, forming oxygen vacancies due to charge compensation. The oxygen vacancies promote material migration and coalescence of the particles, leading to the grain growth and densification. Co-additions with Fe_2O_3 and M_2O_5 (M = Nb, Sb, Ta) have also been performed to explore preparation of electroconductive and dense SnO_2-based ceramics for targeted compositions of $Sn_{0.98-y}Fe_{0.02}M_yO_2$ with y = 0.00 − 0.04. The co-additions with $y < 0.02$ lead to dense and insulating ceramics by firing at 1673 K while those with $y \geq 0.02$ lead to non-densified bulks. These results can be explained by charge compensation between Fe^{3+} and M^{5+} (M = Nb, Sb, Ta) ions co-doped into the Sn^{4+} sites of the rutile-type structure.

1. Introduction

Tin dioxide, SnO_2, is a wide-gap insulator with a rutile-type structure and becomes an n-type conductor when oxygen vacancies or doped pentavalent cations such as Sb^{5+} are included in the structure [1]. The SnO_2-based semiconducting materials are widely used as transparent conducting films or porous gas sensors. The ceramic form has been expected for applications to electrodes, varistors, or thermoelectric materials at high temperatures as described below.

It is well known that pure SnO_2 powder is hard to be densified by normal firing method. Various SnO_2-based ceramics were prepared by firing with an additive such as CuO [2-5], CoO [6-13], MnO_2 [7], and ZnO [14] as a sintering agent for applications to electrodes or varistors. Several ceramics were also prepared by co-addition of CoO and Fe_2O_3 [15, 16] or ZnO and Fe_2O_3 [17]. The densification was promoted by a liquid phase formed during the firing with CuO [2-5] or by oxygen vacancies formed due to charge compensation when the Sn^{4+} sites were doped with lower valency cations such as Co^{2+} [6, 7, 9, 12], Mn^{2+} [7], Zn^{2+} [14], or Fe^{3+} together with Co^{2+} [16] or Zn^{2+} [17]. To investigate the thermoelectric properties [18-24], several SnO_2-

[*1] Corresponding author.
[*2] Graduated in 2020.

based ceramics were prepared by spark plasma sintering (SPS) method [21-23] or by firing with an additive CuO as a sintering agent [24]. The SPS method is effective for rapid preparation of dense ceramics but it needs the exclusive equipment.

On the other hand, the firing of compacts with a sintering agent is a simple and convenient method to prepare dense ceramics. As described above, although several additives were used as sintering agents to prepare dense SnO_2-based ceramics, use of Fe_2O_3 as a single additive has not been reported. Since Fe_2O_3 is a common oxide and easily handled, it is worth investigating the effect of Fe_2O_3 as a single additive to prepare dense SnO_2-based ceramics. Chemani *et al*. [25] reported the influence of Fe_2O_3 additive on the microstructural development of SnO_2, but dense SnO_2-based ceramics were not prepared owing to lower firing temperatures of 1273 K − 1473 K.

In this study, Fe_2O_3-added SnO_2 compacts have been fired at high temperatures of 1473 K − 1673 K to investigate the densification of the samples. It is reported that the firing with Fe_2O_3 addition brings about doping of Fe^{3+} ions into Sn^{4+} sites of the rutile-type structure to form oxygen vacancies due to charge compensation and leads to grain growth and densification of the compacts. Co-additions with Fe_2O_3 and M_2O_5 (M = Nb, Sb, Ta) have also been performed aiming to prepare electroconductive and dense SnO_2-based ceramics.

2. Experiments

Powder reagents of SnO_2 (purity ≥ 99.9 %, Kojundo chemical), Fe_2O_3 (purity ≥ 99.9 %, Wako Pure Chemical), Nb_2O_5 (purity ≥ 99.9 %, Wako Pure Chemical), Sb_2O_5 (purity ≥ 99.9 %, Kojundo chemical), and Ta_2O_5 (purity ≥ 99.9 %, Wako Pure Chemical) were used. For preparation of $Sn_{1-x}Fe_xO_2$, the SnO_2 and Fe_2O_3 powders were weighed stoichiometrically with x = 0.00, 0.001, 0.005, 0.01, 0.02, 0.03, 0.05, and 0.10, and mixed thoroughly with a small amount of ethanol in an agate mortar. The mixed powder was dried and molded into a cylinder with 5 mm or 15 mm in diameter. Each compact was fired at 1473 K − 1673 K for 1 h in air-flow on an alumina boat. For preparation of $Sn_{0.98-y}Fe_{0.02}M_yO_2$ (M = Nb, Sb, Ta), the SnO_2, Fe_2O_3, and M_2O_5 powders were weighed stoichiometrically with y = 0.00, 0.01, 0.02, 0.03, and 0.04, and mixed thoroughly with a small amount of ethanol in an agate mortar. The mixed powder was dried and molded into a cylinder with 5 mm in diameter, and each compact was fired at 1673 K for 1 h in air-flow on an alumina boat.

The bulk density of the fired samples was estimated from the weight and the volume which was calculated from the diameter and the height. The microstructure for the fractured surface of the fired samples was observed by scanning electron microscopy (SEM; JEOL, JSM-6610LA). The fractured samples were washed in deionized water using an ultrasonic washer to remove debris and dried before the SEM observations. The crystalline phases in the fired samples were identified by powder X-ray diffraction (XRD) measurements with CuKα radiation (Rigaku, RINT-Ultima III), and the lattice parameters a and c of the rutile-type structure were calculated by the least-squares method using the observed diffraction angles. The electrical resistance for the fired samples was measured between two points with a distance of about 1 mm using a multimeter (Custom Corporation, CDM-03D).

3. Results and discussion

Figure 1 shows firing temperature dependence of the bulk density for the Fe_2O_3-added SnO_2 samples with x = 0.00, 0.05, and 0.10. The Fe_2O_3-added samples with x = 0.05 and 0.10 are densified by firing at each temperature between 1473 K and 1673 K, and the bulk density becomes higher with increasing firing temperature. On the other hand, the pure SnO_2 compact without Fe_2O_3 addition is not densified by firing at 1673 K and the relative density after the firing is about 50 % for the theoretical density (7.01 $g \cdot cm^{-3}$) [26]. Any weight loss indicating volatilization of the constituent elements is not observed for these samples with x = 0.00, 0.05, and 0.10 even after the re-firing at 1673 K for 1 h in air-flow.

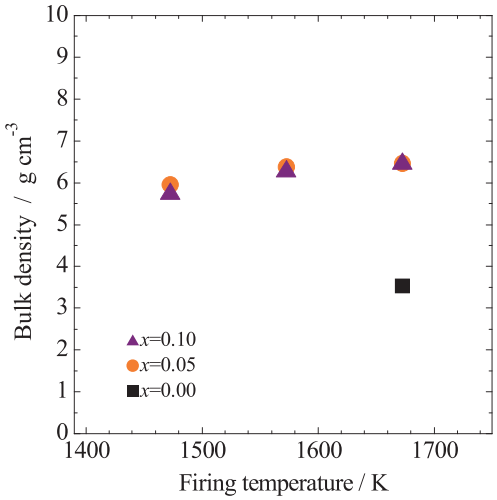

Figure 1 Firing temperature dependence of the bulk density for Fe_2O_3-added SnO_2 samples with atomic ratio x = Fe/(Sn+Fe) = 0.00, 0.05, and 0.10.

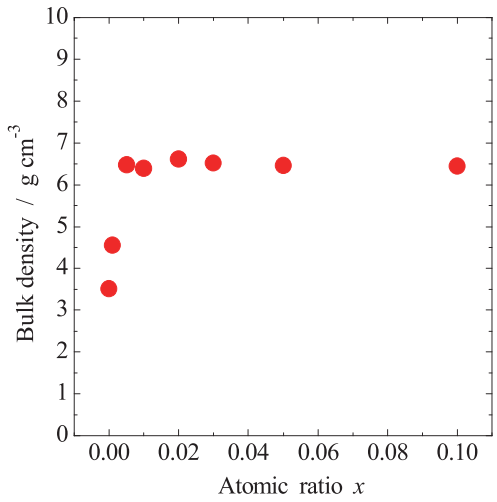

Figure 2 Plots of the bulk density on the atomic ratio x = Fe/(Sn+Fe) for Fe_2O_3-added SnO_2 samples fired at 1673 K for 1 h in air-flow.

Figure 2 shows plots of the bulk density on the atomic ratio x in the range of x = 0.00 − 0.10 for the Fe_2O_3-added SnO_2 samples fired at 1673 K for 1 h in air-flow. The samples with x = 0.005 − 0.10 are well densified by the firing, exhibiting the bulk densities higher than 6.3 $g \cdot cm^{-3}$. It should be noted that the sample even with x = 0.005 is well densified by the firing, but that with x = 0.001 is not densified. The color of the densified bodies with x = 0.005 − 0.10 is dark brown, but the pulverized powders are pale grey to dark grey with increasing x. On the other hand, the colors of the fired bodies with x = 0.00 and 0.001 are white and reddish white, respectively. All the fired bodies with x = 0.00 − 0.10 are electrically insulating at room temperature, because the electrical resistances are beyond the detection limit (40 MΩ) of the multimeter.

Figure 3 shows SEM images for the fractured surfaces of the samples with x = 0.00 − 0.10 after firing at 1673 K for 1 h in air-flow. The sample with x = 0.00 has a porous and non-densified microstructure consisting of small particles with sub-micrometers to a few micrometers in size, whereas the samples with x = 0.005 − 0.10 have well-densified microstructures consisting of grains with a few micrometers to about 10 micrometers in size. The sample with x = 0.001 is not densified and is porous but consists of grains combined each other. The small holes observed for the samples with x = 0.02 − 0.10 are considered to be traces of Sn-doped Fe_2O_3 ($Fe_{2-z}Sn_zO_3$) particles probably removed by washing using the ultrasonic washer before SEM observations. The $Fe_{2-z}Sn_zO_3$ phase is confirmed by XRD results described in the next paragraph.

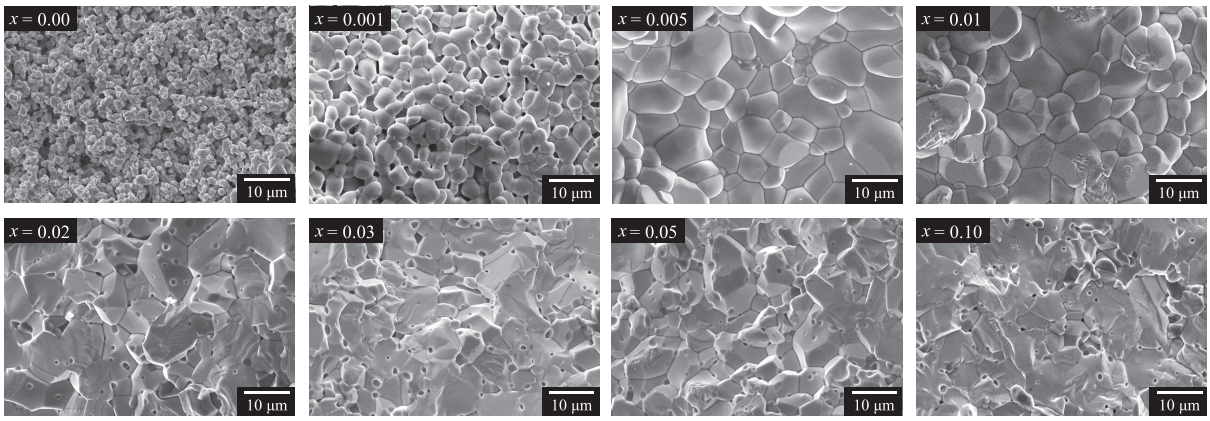

Figure 3 SEM images for the fractured surfaces of Fe_2O_3-added SnO_2 samples with atomic ratio x = Fe/(Sn+Fe) = 0.00, 0.001, 0.005, 0.01, 0.02, 0.03, 0.05, and 0.10 fired at 1673 K for 1 h in air-flow.

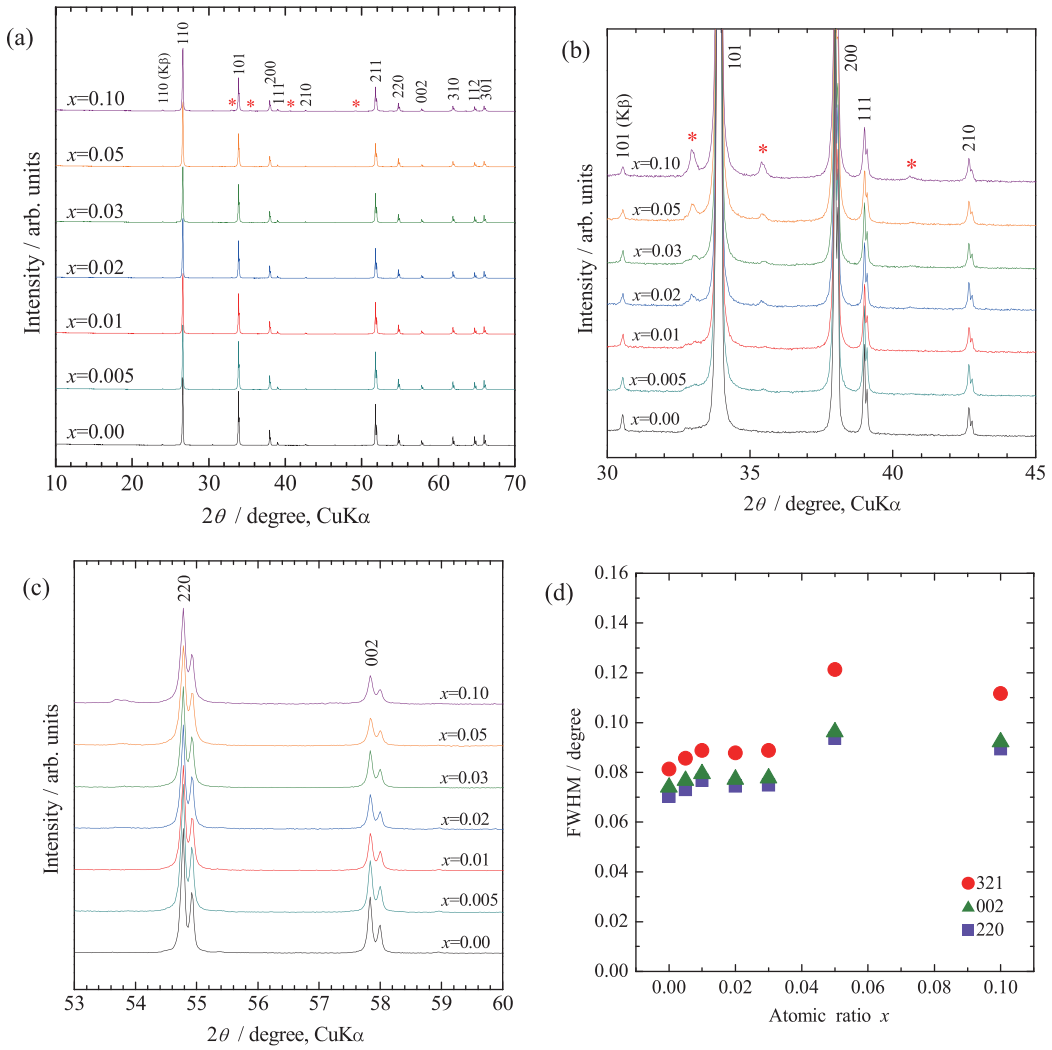

Figure 4 (a) XRD patterns for Fe_2O_3-added SnO_2 samples with atomic ratio x = Fe/(Sn+Fe) = 0.00, 0.005, 0.01, 0.02, 0.03, 0.05, and 0.10 fired at 1673 K for 1 h in air-flow. Asterisks denote diffraction peaks from $Fe_{2-z}Sn_zO_3$ [27]. (b) Magnification of the XRD patterns to 2θ range of 30° – 45°. (c) Magnification of the XRD patterns to 2θ range of 53° – 60°. The indices 220 and 002 denote diffraction peaks from the tetragonal rutile-type structure. (d) Plots of the full width at half maximum (FWHM) for the diffraction peaks 220, 002, and 321 (2θ ~ 78.72°) on the atomic ratio x = Fe/(Sn+Fe).

Figure 4(a) shows XRD patterns for the samples with $x = 0.00 - 0.10$ after firing at 1673 K for 1 h in air-flow. All the XRD patterns are indexed with diffraction peaks for the rutile-type SnO_2 [26], but extremely weak peaks from Sn-doped Fe_2O_3 ($Fe_{2-z}Sn_zO_3$) [27] are additionally observed at the 2θ angles marked by asterisks for the samples with $x = 0.02 - 0.10$ as shown in Figure 4(b). This indicates that extremely slight amount of $Fe_{2-z}Sn_zO_3$ exists locally as another stable phase besides the main rutile-type phase after the firing. It is supposed that the small holes observed in the SEM images for the samples with $x = 0.02 - 0.10$ are the traces of small particles of the $Fe_{2-z}Sn_zO_3$ phase. The residue of the $Fe_{2-z}Sn_zO_3$ phase may be due to rapid densification process during the firing. Figure 4(c) shows a magnification of the XRD patterns to a 2θ range of $53^\circ - 60^\circ$, which exhibits two diffraction peaks 220 and 002 for the rutile-type structure. It should be noted that any peak shifts are not observed for the both diffraction peaks with increasing x from $x = 0.00$ to $x = 0.10$. Indeed, the calculated lattice parameters a and c of the tetragonal rutile-type structure are constant for all the samples with $x = 0.00 - 0.10$, indicating $a = 4.7359(3)$ Å and $c = 3.1855(3) - 3.1860(3)$ Å, respectively. Although the lattice parameters are constant for all the samples, it is considered that the Fe ions are doped into the rutile-type structure successively with increasing x because the peak intensities of the $Fe_{2-z}Sn_zO_3$ phase are extremely low even for the samples with $x = 0.05$ and 0.10. Based on the ionic radius [28], it can be considered that the Sn^{4+} ions (ionic radius: 0.69 Å) are substituted with Fe^{3+} ions with a high spin state (ionic radius: 0.645 Å) rather than Fe^{3+} with a low spin state (ionic radius: 0.55 Å). The previous paper on ^{57}Fe Mössbauer spectra of the rutile-type $Sn_{0.95}Fe_{0.05}O_2$ sample fired at 1423 K reported that the Fe ions are doped into the Sn sites as high spin Fe^{3+} [29]. Figure 4(d) shows plots of the full width at half maximum (FWHM) for the diffraction peaks 220, 002, and 321 on the atomic ratio x. Although there is some dispersion for the values, the tendency of the increase in the FWHM with increasing x may suggest distortion of lattice planes due to doping of the Fe ions into the Sn sites.

The densification mechanism for the Fe_2O_3-added SnO_2 is briefly described in this paragraph. The doping of Fe^{3+} ions into the Sn^{4+} sites brings about the formation of oxygen vacancies to compensate the lack of positive charges in the structure. The oxygen vacancies formed during the firing promote diffusion of oxide ions and material migration leading to coalescence of the particles and grain growth to densify the $Sn_{1-x}Fe_xO_2$ bulks. The similar mechanism was described in the previous papers for the other SnO_2-based ceramics prepared with a sintering additive such as CoO [6, 7, 9, 12], MnO_2 [7], or ZnO [14] and with two additives such as CoO and Fe_2O_3 [16] or ZnO and Fe_2O_3 [17].

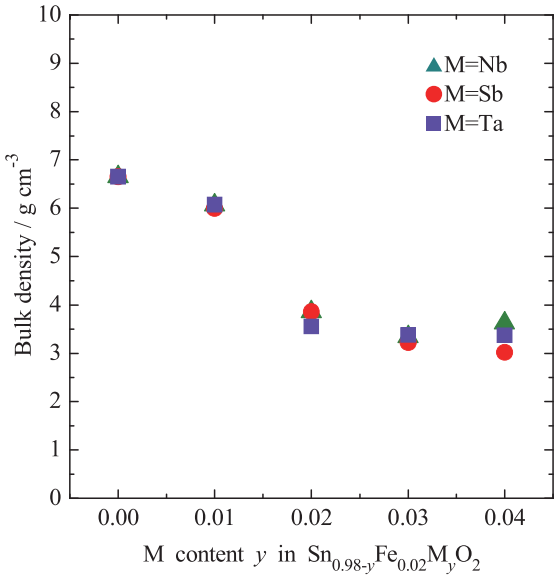

Figure 5 Plots of the bulk density on the M content y in targeted compositions $Sn_{0.98-y}Fe_{0.02}M_yO_2$ (M = Nb, Sb, Ta). The samples co-added with Fe_2O_3 and M_2O_5 (M = Nb, Sb, Ta) were fired at 1673 K for 1 h in air-flow.

In order to explore preparation of electroconductive and dense SnO_2-based ceramics, co-addition of Fe_2O_3 and pentavalent metallic oxide of Nb_2O_5, Sb_2O_5, or Ta_2O_5 to SnO_2 has been performed expecting that the Fe_2O_3 and M_2O_5 (M = Nb, Sb, Ta) work as the sintering agent and the electron dopant, respectively. Figure 5 shows plots of the bulk density for the samples fired at 1673 K on the M content y in the targeted compositions of $Sn_{0.98-y}Fe_{0.02}M_yO_2$ (M = Nb, Sb, Ta; y = 0.00 − 0.04). It is clearly seen for M = Nb, Sb, Ta that the samples with y = 0.00 and 0.01 are densified exhibiting the bulk densities higher than 6.0 $g \cdot cm^{-3}$ whereas those with $y \geq 0.02$ are not densified exhibiting the bulk densities lower than 3.9 $g \cdot cm^{-3}$. Any weight loss indicating sublimation of the constituent elements is not observed after the re-firing at 1673 K for the fired bodies of M = Nb, Sb, Ta. The electrical resistances measured using the multimeter are beyond the detection limit (40 MΩ) for all the fired samples except for $Sn_{0.98-y}Fe_{0.02}Sb_yO_2$ with y = 0.03 and 0.04. The XRD patterns indicate that all the fired samples of M = Nb, Sb, Ta are composed of the rutile-type single phase except for the samples with y = 0.03 and 0.04 of M = Ta, which include small amounts of Ta_2O_5 not dissolved in the rutile-type phase. The y dependence of the bulk density shown in Figure 5 can be explained by charge compensation mechanism between Fe^{3+} and M^{5+} ions co-doped into the Sn^{4+} sites of the rutile-type structure. For the fired samples with y = 0.00 and 0.01 of M = Nb, Sb, Ta, oxygen vacancies are generated but electron carriers are not generated because the number of Fe^{3+} ions doped in the structure is larger than that of M^{5+} ions, leading to the formation of the densified and highly resistive ceramics. For y = 0.02 of M = Nb, Sb, Ta, neither oxygen vacancies nor electron carriers are generated in the structure because the number of doped Fe^{3+} ions is equal to that of M^{5+} ions, leading to the formation of the non-densified and highly resistive bulks. For $y > 0.02$ of M = Nb, Sb, Ta, oxygen vacancies are no longer generated, leading to the formation of the non-densified bulks. Therefore, the preparation of electroconductive and dense SnO_2-based ceramics has not been successful by the present co-additions of Fe_2O_3 and M_2O_5, owing to charge compensation between Fe^{3+} and M^{5+} ions doped in the Sn^{4+} sites. However, these results are consistent with the aforementioned result that the Fe ions are doped as Fe^{3+} in the Sn^{4+} sites forming oxygen vacancies, leading to the densification of the Fe-doped SnO_2.

4. Conclusions

Dense SnO_2-based ceramics have been prepared by firing Fe_2O_3-added SnO_2 compacts with atomic ratio x = Fe/(Sn+Fe) = 0.005 − 0.10 at 1673 K for 1 h in air-flow. The successive doping of Fe^{3+} ions into the Sn^{4+} sites of the rutile-type structure with increasing x has been deduced on the basis of the XRD patterns, the FWHM of the diffraction peaks, and the comparison of the ionic radii. The doping of Fe^{3+} ions into the Sn^{4+} sites results in oxygen vacancies to compensate the lack of positive charges in the structure, and the oxygen vacancies promote diffusion of oxide ions and material migration, leading to coalescence of particles, grain growth, and densification of the fired bodies. The firing of SnO_2 compacts co-added with Fe_2O_3 and M_2O_5 (M = Nb, Sb, Ta) also brings about charge compensation between Fe^{3+} and M^{5+} (M = Nb, Sb, Ta) doped in the rutile-type structure, preventing simultaneous realization of densification and electron doping.

Acknowledgments

This research did not receive any specific grant from funding agencies in the public, commercial, or not-for-profit sectors.

References

[1] P. A. Cox, The electronic structure and chemistry of solids, Oxford University Press Inc., New York, 1987.

[2] M. Zaharescu, S. Mihaiu, S. Zuca, K. Matiasovsky, Contribution to the study of SnO_2-based ceramics: Part I High-temperature interactions of tin (IV) oxide with antimony (III) oxide and copper (II) oxide, J. Mater. Sci. 26 (1991) 1666 − 1672.

[3] S. Zuca, M. Terzi, M. Zaharescu, K. Matiasovsky, Contribution to the study of SnO_2-based ceramics: Part II Effect of various oxide additives on the sintering capacity and electrical conductivity of SnO_2, J. Mater. Sci. 26 (1991) 1673 − 1676.

[4] N. Dolet, J.-M. Heintz, M. Onillon, J.-P. Bonnet, Densification of $0.99SnO_2$-0.01CuO mixture: Evidence for liquid phase sintering, J. Eur. Ceram. Soc. 9 (1992) 19 − 25.

[5] N. Dolet, J. M. Heintz, L. Rabardel, M. Onillon, J. P. Bonnet, Sintering mechanism of $0.99SnO_2$-0.01CuO mixtures, J. Mater. Sci. 30 (1995) 365 − 368.

[6] S. A. Pianaro, P. R. Bueno, E. Longo, J. A. Varela, A new SnO_2-based varistor system, J. Mater. Sci. Lett. 14 (1995) 692 − 694.

[7] J. A. Cerri, E. R. Leite, D. Gouvêa, E. Longo, J. A. Varela, Effect of cobalt (II) oxide and manganese (IV) oxide on sintering of tin (IV) oxide, J. Am. Ceram. Soc. 79 (1996) 799 − 804.

[8] S. A. Pianaro, P. R. Bueno, P. Olivi, E. Longo, J. A. Varela, Effect of Bi_2O_3 addition on the microstructure and electrical properties of the $SnO_2 \cdot CoO \cdot Nb_2O_5$ varistor system, J. Mater. Sci. Lett. 16 (1997) 634 − 638.

[9] J. A. Varela, J. A. Cerri, E. R. Leite, E. Longo, M. Shamsuzzoha, R. C. Bradt, Microstructural evolution during sintering of CoO doped SnO_2 ceramics, Ceram. Int. 25 (1999) 253 − 256.

[10] A. B. Glot, R. Bulpett, A. I. Ivon, P. M. Gallegos-Acevedo, Electrical properties of SnO_2 ceramics for low voltage varistors, Physica B 457 (2015) 108 − 112.

[11] M. Maleki Shahraki, M. A. Bahrevar, S. M. S. Mirghafourian, A. B. Glot, Novel SnO_2 ceramic surge absorbers for low voltage applications, Mater. Lett. 145 (2015) 355 − 358.

[12] S. Tominc, A. Rečnik, Z. Samardžija, G. Dražić, M. Podlogar, S. Bernik, N. Daneu, Twinning and charge compensation in Nb_2O_5-doped SnO_2-CoO ceramics exhibiting promising varistor characteristics, Ceram. Int. 44 (2018) 1603 − 1613.

[13] A. N. Bondarchuk, A. B. Glot, A. R. Velasco-Rosales, Effects of Sb and Nb dopants on electrical and microstructural properties of low-voltage varistor ceramics based on SnO_2, Ceram. Int. 44 (2018) 7844 − 7850.

[14] I. Saadeddin, H. S. Hilal, B. Pecquenard, J. Marcus, A. Mansouri, C. Labrugere, M. A. Subramanian, G. Campet, Simultaneous doping of Zn and Sb in SnO_2 ceramics: Enhancement of electrical conductivity, Solid State Sci. 8 (2006) 7 − 13.

[15] A. C. Antunes, S. R. M. Antunes, A. J. Zara, S. A. Pianaro, E. Longo, J. A. Varela, Effect of Fe_2O_3 doping on the electrical properties of a SnO_2 based varistor, J. Mater. Sci. 37 (2002) 2407 − 2411.

[16] R. Parra, C. M. Aldao, J. A. Varela, M. S. Castro, The role of oxygen vacancies on the microstructure development and on the electrical properties of SnO_2-based varistors, J. Electroceramics 14 (2005) 149 − 156.

[17] R. Parra, J. A. Varela, C. M. Aldao, M. S. Castro, Electrical and microstructural properties of (Zn, Nb, Fe) -doped SnO_2 varistor system, Ceram. Int. 31 (2005) 737 − 742.

[18] T. Tsubota, T. Ohno, N. Shiraishi, Y. Miyazaki, Thermoelectric properties of $Sn_{1-x-y}Ti_ySb_xO_2$ ceramics,

J. Alloy. Compd. 463 (2008) 288 − 293.

[19] S. Yanagiya, N. V. Nong, J. Xu, M. Sonne, N. Pryds, Thermoelectric properties of SnO_2 ceramics doped with Sb and Zn, J. Electron. Mater. 40 (2011) 674 − 677.

[20] S. Yanagiya, N. V. Nong, M. Sonne, N. Pryds, Thermoelectric properties of SnO_2-based ceramics doped with Nd, Hf or Bi, AIP Conf. Proc. 1449 (2012) 327 − 330.

[21] S. Yanagiya, S. Furuyama, I. Uriya, M. Takeda, Thermoelectric properties of SnO_2 ceramics codoped with Sb and Zn prepared by reactive spark plasma synthesis followed by thermal treatment, Sens. Mater. 27 (2015) 917 − 924.

[22] T. T. Xuan Vo, T. N. Ha Le, Q. N. Pham, C. Byl, D. Dragoe, M.-G. Barthés-Labrousse, D. Bérardan, N. Dragoe, Preparation and study of the thermoelectric properties of nanocrystalline $Sn_{1-x}Ta_xO_2$ ($0 \leq x \leq 0.04$), Phys. Status Solidi A 212 (2015) 2776 − 2784.

[23] K. Rubenis, S. Populoh, P. Thiel, S. Yoon, U. Müller, J. Locs, Thermoelectric properties of dense Sb-doped SnO_2 ceramics, J. Alloy. Compd. 692 (2017) 515 − 521.

[24] T. Tsubota, S. Kobayashi, N. Murakami, T. Ohno, Improvement of thermoelectric performance for Sb-doped SnO_2 ceramics material by addition of Cu as sintering additive, J. Electron. Mater. 43 (2014) 3567 − 3573.

[25] H. Chemani, B. Chemani, Influence of the sintering additive (Fe_2O_3) to the morphological and microstructural development of SnO_2 ceramic powders, Asian J. Chem. 24 (2012) 5324 − 5328.

[26] W. H. Baur, Über die verfeinerung der kristallstrukturbestimmung einiger vertreter des rutiltyps: TiO_2, SnO_2, GeO_2 und MgF_2, Acta Cryst. 9 (1956) 515 − 520.

[27] F. J. Berry, C. Greaves, J. G. McManus, M. Mortimer, G. Oates, The structural characterization of tin- and titanium-doped α-Fe_2O_3 prepared by hydrothermal synthesis, J. Solid State Chem. 130 (1997) 272 − 276.

[28] R. D. Shannon, Revised effective ionic radii and systematic studies of interatomic distances in halides and chalcogenides, Acta Cryst. A32 (1976) 751 − 767.

[29] C. B. Fitzgerald, M. Venkatesan, A. P. Douvalis, S. Huber, J. M. D. Coey, T. Bakas, SnO_2 doped with Mn, Fe or Co: Room temperature dilute magnetic semiconductors, J. Appl. Phys. 95 (2004) 7390 − 7392.

受理日：2022年11月９日